Green Chemistry

Volume 1 | Number 1 | Jan 2013 | Pages 1–100

Green Chemistry

Cutting-edge research for a greener sustainable future

www.rsc.org/greenchem

ROYAL SOCIETY OF CHEMISTRY

www.rsc.org/greenchem

High coercivity FePt $L1_0$ nanoparticles were prepared by ball-milling in a solvent-free one pot synthesis at low temperature.

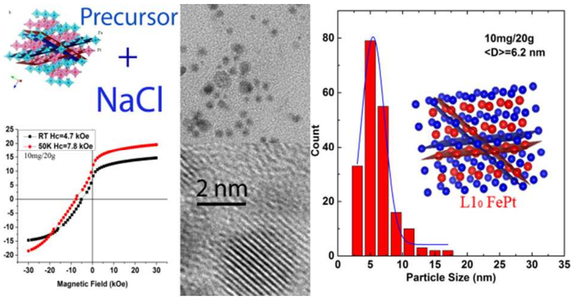

Cite this: DOI: 10.1039/c0xx00000x

www.rsc.org/xxxxxx

ARTICLE TYPE

A Low Temperature and Solvent-free Direct Chemical Synthesis of $L1_0$ FePt Nanoparticles with Size Tailoring

X. C. Hu, [a] ***E. Agostinelli,*** [b] ***C. Ni,*** [a] ***G. C. Hadjipanayis,*** [c] ***and A. Capobianchi.*** *[b]

Received (in XXX, XXX) Xth XXXXXXXXX 20XX, Accepted Xth XXXXXXXXX 20XX
DOI: 10.1039/b000000x

FePt alloy in the high magnetic anisotropy $L1_0$ phase is one of the most promising magnetic materials in many applications, including ultra high-density magneto recording. A new green chemical approach to synthesize magnetically hard $L1_0$ FePt nanoparticles is described in this paper by using crystalline saline complex hexaaquairon(II)hexachloroplatinate, $[Fe(H_2O)_6]PtCl_6$ as the precursor. The crystal structure of this complex shows alternate layers of Fe and Pt atoms. After ball milling, annealing at 400 °C in reducing atmosphere leads to the direct formation of FePt nanoparticles in the highly ordered $L1_0$ phase. This method is a green synthesis due to the low temperature for phase transformation, and the absence of organic solvents or surfactants in the reaction. Indeed the milling step is performed using NaCl as media, which can be easily removed with water. By varying the precursor/NaCl ratio, particles with size in the range of 6.2 – 13.2 nm were obtained. With the decrease of particle size, the room temperature coercivity of FePt nanoparticles also decreased from 10.9 kOe to 4.7 kOe.

Introduction

Magnetic nanoparticles (NPs) have been attracting a great attention recently, due to their potential application in different fields such as data storage[1], permanent magnetic nanocomposites[2, 3] and biomedicine.[4] Binary alloys, where the two metal atoms are chemically ordered in alternate planes within a face centered tetragonal (fct) structure, crystallize in the so-called $L1_0$ phase. In $L1_0$ alloys, a tetragonal cell is formed whenever the two metals have atoms with very dissimilar dimension. Magnetically hard $L1_0$ alloys are formed from the combination of big atoms, such as Pt or Pd, and smaller ferromagnetic atoms, such as Fe or Co. Due to the spin-orbit coupling between the alternate planes, a very high magnetocrystalline anisotropy is generated; for this reason such materials have a huge importance in magnetic applications. In particular, in recent years, $L1_0$ FePt nanoparticles have been considered as one of the most promising candidates for future magnetic recording media with areal density larger than 1 Tbit/in^2 due to the large magnetic anisotropy energy of 7×10^7 erg/cc[5, 6] (which allows stable ferromagnetic particles with size as small as 2.8 nm), their resistance to oxidization and their stability at room temperature.[7]

Currently, there are two major methods for preparation of high quality $L1_0$ FePt phase. One method consists in depositing FePt films through physical vapour deposition (PVD) techniques such as sputtering. Usually, in order to favour the epitaxial growth of FePt films, substrates such as MgO (001), with a well-defined crystallographic orientation, are used.[7-9] In this case, an island growth is usually observed with island sizes as large as 50-100 nm, which is certainly undesirable for high density magnetic recording. Moreover, to get the $L1_0$ structure, very high substrate temperatures up to 800 °C are used, and this is detrimental for the environment, since the process is energy consuming. Another method, widely reported in the literature, is the chemical synthesis of FePt nanoparticles based on the reduction of mixed metal salts ($Fe(CO)_5$ and $Pt(acac)_2$) in the presence of a long chain carboxylic acid and primary amines in organic solvents, as first published by Sun et al.[10] To obtain nanoparticles, organic solvents and surfactants are used. Considering also the presence of the harmful and hazardous compound $Fe(CO)_5$, this synthesis is not environmentally friendly. Furthermore, the as-made FePt NPs are in the fcc phase and more energy (annealing at temperature higher than 650°C) is needed for the phase transformation from the fcc to the fct $L1_0$ phase, which usually introduces agglomeration and sintering of the particles.[11-13] For this reason, many attempts have been made in order to decrease the annealing temperature required for the phase transformation. Nakaya et al.[14] reported a phase transformation temperature of 300°C, but a strongly reducing atmosphere, such as pure H_2, was used. Another method reported the usage of metals as catalysts for the fcc-fct transformation.[15] Other new chemical routes for direct synthesis of $L1_0$ FePt NPs have been recently proposed[16, 17], but the fraction of the ordered phase obtained is usually small.[18].

In our previous letter[19], we reported a direct chemical synthesis of FePt NPs in $L1_0$ phase. In the present work, we report a new environmentally friendly approach for the direct synthesis of FePt NPs, starting from the same polycrystalline molecular compound $[Fe(H_2O)_6]PtCl_6$, where Fe and Pt atoms are arranged on alternating planes resembling the chemical order they have in the fct $L1_0$ structure. In this green synthesis method, unlike the previously reported method, no organic solvents are used but only

$FeCl_2$ and $H_2PtCl_6(H_2O)$ in stoichiometric amounts to fabricate precursors, environmentally friendly and low cost NaCl to mill and water to wash. Furthermore, also in this case the phase transformation temperature to obtain a highly ordered, magnetically hard phase was reduced by about 250 °C as compared to the annealing needed in the Sun's synthesis procedure.

Experimental

Synthesis of $[Fe(H_2O)_6]PtCl_6$

All reagents were purchased from Aldrich. To synthesize the starting polycrystalline complex $[Fe(H_2O)_6]PtCl_6$, a 0.5 M solution containing equal atomic concentration of $H_2PtCl_6{\cdot}6H_2O$ and $FeCl_2{\cdot}H_2O$ was prepared using distilled water. The acidity of the solution of $H_2PtCl_6{\cdot}6H_2O$ (pH = 1) prevented the Fe^{2+} to Fe^{3+} oxidation. The reaction begun immediately after mixing the reactants, with the production of HCl gas, as proved by the white AgCl precipitate obtained when the vapour was reacted with an $AgNO_3$ solution. After a slow evaporation of the solvent at room temperature a yellow precipitate of hexagonal crystals was collected. The only safe way to increase the reaction velocity was to remove the vapour by a nitrogen flow or to work under vacuum conditions (10^{-3} mbar). Since both $H_2PtCl_6{\cdot}6H_2O$ and $Fe(H_2O)_6PtCl_6$ are thermo labile compounds, the temperature was kept under 50°C to avoid the reduction of Pt. The hexagonal crystals of $[Fe(H_2O)_6]PtCl_6$ were then purified by recrystallization in ethyl alcohol.

Synthesis of $L1_0$ FePt NPs

The precursor $Fe(H_2O)_6PtCl_6$ was mixed with NaCl in different proportion (50mg/20g, 25mg/20g, 10mg/20g) and milled in a planetary milling using a jar (50 mm diameter; 50 mm height) with 6 ZrO balls (10 mm diameter) for 5 h at 250 rpm. After milling, a uniform light-yellow mixture containing NaCl and isolated nanocrystals of the precursor was obtained. Then, the powder was heated (heating rate = 5 K/min) up to 400 °C in a horizontal furnace under a reducing atmosphere of 0.1 L/min flow of 5% H_2 and 95% Ar. Then the samples were kept at the final temperature for 2 h. The following reduction reaction takes place:

$$[Fe(H_2O)_6]PtCl_6 + 3H_2 \rightarrow FePt(L1_0) + 6H_2O + 6HCl.$$

After cooling down, a pale-grey powder was collected, and washed with water. The $L1_0$ FePt NPs were collected by magnetic separation using a magnetic field generated by an electromagnet, until the test on the washing water with $AgNO_3$, very sensitive to the presence of Cl^-, became negative. The theoretical mass yield of our method is 43% (after elimination of H_2O and Cl from the precursor). Actually, we observed a yield of 35%, due to the loss of material during the washing step.

Characterization

The FePt particle size and size distribution were determined by transmission electron microscopy (TEM) (JEOL JEM-2010) with a voltage of 200 keV. The crystal structure was determined by both selected area electron diffraction (SEAD) and X-ray diffraction (XRD) patterns (Ultima IV with Cu Kα radiation) using a conventional θ-2θ plane reflection geometry. Magnetic properties were measured by a Versa Lab vibrating sample magnetometer (VSM) (Quantum Design)

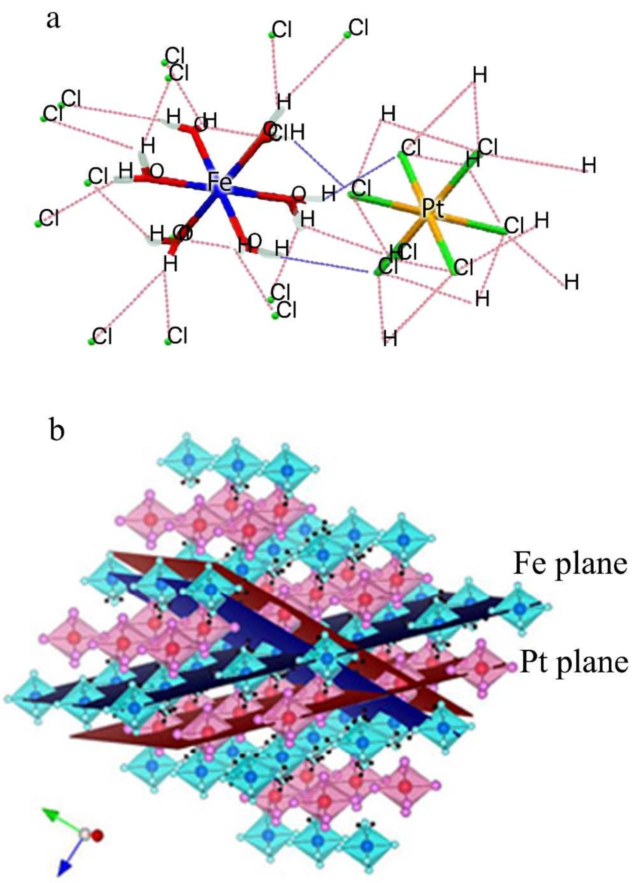

Figure 1. (a) Octahedral ions of Fe and Pt, (b) crystal structure of $Fe(H_2O)_6PtCl_6$ where alternate planes of Fe and Pt are visible.

Results and discussion

In our previous letter[19], we proved that the chemical reduction of a layered precursor such as $[Fe(H_2O)_6]PtCl_6$ brings to a highly ordered $L1_0$ FePt phase. Single crystals of $[Fe(H_2O)_6]PtCl_6$, characterized by a perfect hexagonal shape, were obtained by re-crystallization of the crude product (see experimental section for the synthesis). The crystal structure of $[Fe(H_2O)_6]PtCl_6$ has been reported.[20] A view of the crystal packing is shown in Fig.1, representing octahedral $[PtCl_6]^{2-}$ and $[Fe(H_2O)_6]^{2+}$ ions linked together through a network of hydrogen bonds.

Two different sets of alternating Fe and Pt atomic planes can be distinguished along the [001] and [011] directions, respectively. By reducing at 400 °C, the FePt alloy is obtained in the $L1_0$ phase.

As reported in the literature, the annealing temperature for initiating the fcc to fct transition in a bulk FePt system is about 800-850 °C, and it can be decreased to around 650°C in nanoparticles prepared by chemical route.[11-13] In sputtered FePt films a transition at lower temperature (T = 500°C) was observed.[21] Nakaya et al.[14] reported that the use of pure H_2

during the annealing treatment leads to a decrease of the transformation temperature to 300°C, attributing this result to the higher mobility of Fe and Pt atoms due to hydrogen diffusion in interstitial sites. A more remarkable temperature reduction (down to 275°C) was observed in FePt epitaxial films obtained by the alternate layer growth of Fe and Pt.[22] In both films and nanoparticles the starting alloy completes the phase transformation in a temperature range and a well-defined transition temperature is hardly identified. The presence of random starting configurations in particle systems and different degrees of order achieved in the different preparation processes can explain the spread of transition temperatures reported in the literature. Indeed, it is generally agreed that a higher percentage of chemically ordered Pt and Fe atoms in the starting material is associated with a decrease of the phase transformation temperature.[23] Song and co-workers published a work about the utilization of a single organometallic compound $(CO)_3Fe(-Ph_2PCH_2PPh_2)(-CO)PtCl_2$ containing iron and platinum atoms inside the same molecule.[24] After reduction and annealing at 550 °C partially ordered FePt NPs were observed. On the contrary, we successfully obtained the fct FePt NPs at an annealing temperature as low at 400 °C due to the ordered starting precursor. From a thermodynamic point of view, in our synthesis an energetically favoured starting point for the transformation to the tetragonal phase is present. Fig 2 shows a qualitative thermodynamic diagram for the fcc/fct phase transformation for both amorphous and ordered crystalline precursors. In the case of an amorphous precursor (Fig. 2 a) a low energy is needed for the salt reduction (the reduction easily happens in solution, as in the Sun's synthesis).[10] This step brings to the crystalline but chemically disordered fcc phase. However, a much higher energy (proportional to the decrease of the entropy S) is required to induce the disorder-order transition where the atoms re-arrange by diffusion onto alternate single metal layers. When using a crystalline layered precursor, the energy balance for the reaction is more favourable, the entropic contribution is minimized (see Fig 2b) and less energy is required for Fe and Pt reduction (the reduction in this case occurring in the solid/gas interaction). Thermal analysis (TGA-DTA) and structural data of the starting salt have been reported in our previous works.[19-20]

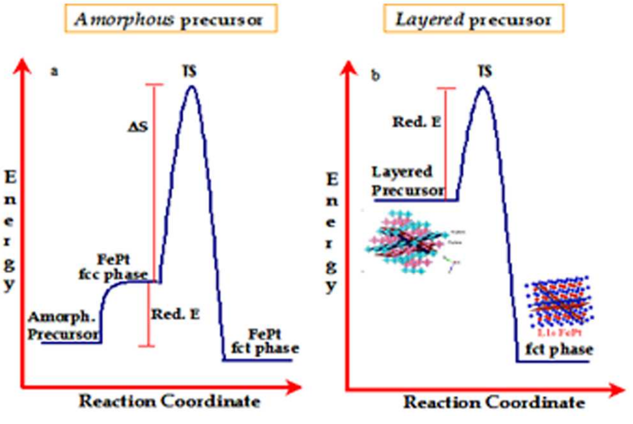

Figure 2. Qualitative thermodynamic reaction paths in the case of amorphous or crystalline precursors.

The main difference of the synthesis proposed in this paper compared to the synthesis already discussed[19] is the type of additive used in the ball milling step. In the previous synthesis the intermediate products were FePt NPs mixed with silica oxide, which had to be eliminated using HF, and therefore, the procedure could not be considered environmentally friendly. In the present synthesis method we replaced SiO_2 microparticles by NaCl.

NaCl was chosen because its crystals are hard enough to break the crystals of the starting salt without destroying the crystalline structure. Moreover, after heating and cooling procedures in reducing atmosphere, NaCl can be easily removed using deionized water and the $L1_0$ FePt nanoparticles can be collected.

To investigate the influence of different precursor/NaCl ratio, one set of FePt NPs was fabricated as listed in the summary table, where structural and magnetic properties are reported.

Label	S50	S25	S10
Precursor/NaCl ratio	50mg/20g	25mg/20g	10mg/20g
Ms at RT (emu/g)	35.4	20.6	14.7
Hc at RT(kOe)	10.9	5.2	4.7
Mr/Ms at RT	0.67	0.59	0.56
Average Size (nm)	13.2	12.1	6.2
Size Standard Deviation (nm)	5.6	4.6	2.6

The XRD patterns reported in Fig 3 show the presence of the peaks characteristic of the $L1_0$ phase. For sample S50, the characteristic (001), (110), (201) and (112) peaks were easily observed and also the split of peaks (002) and (200), (220) and (202). Both S25 and S10 samples show broader diffraction peaks, probably due to the presence of very small particles. However, the broadening of (200) and (220) reflections can be also attributed to the presence of the $L1_0$ phase.

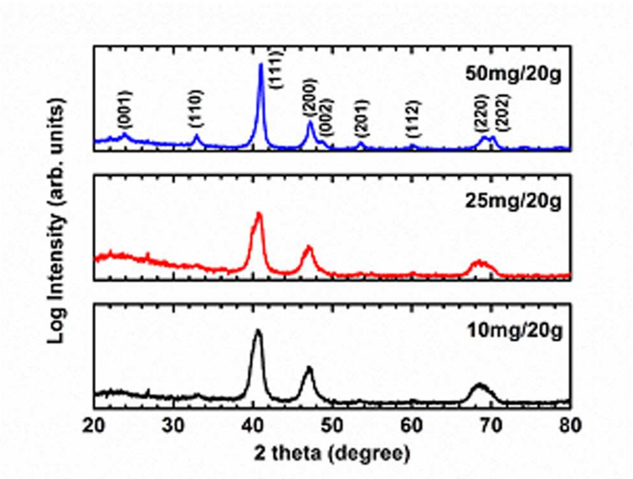

Figure 3. θ-2θ XRD pattern of FePt NPs with different precursor/NaCl ratio

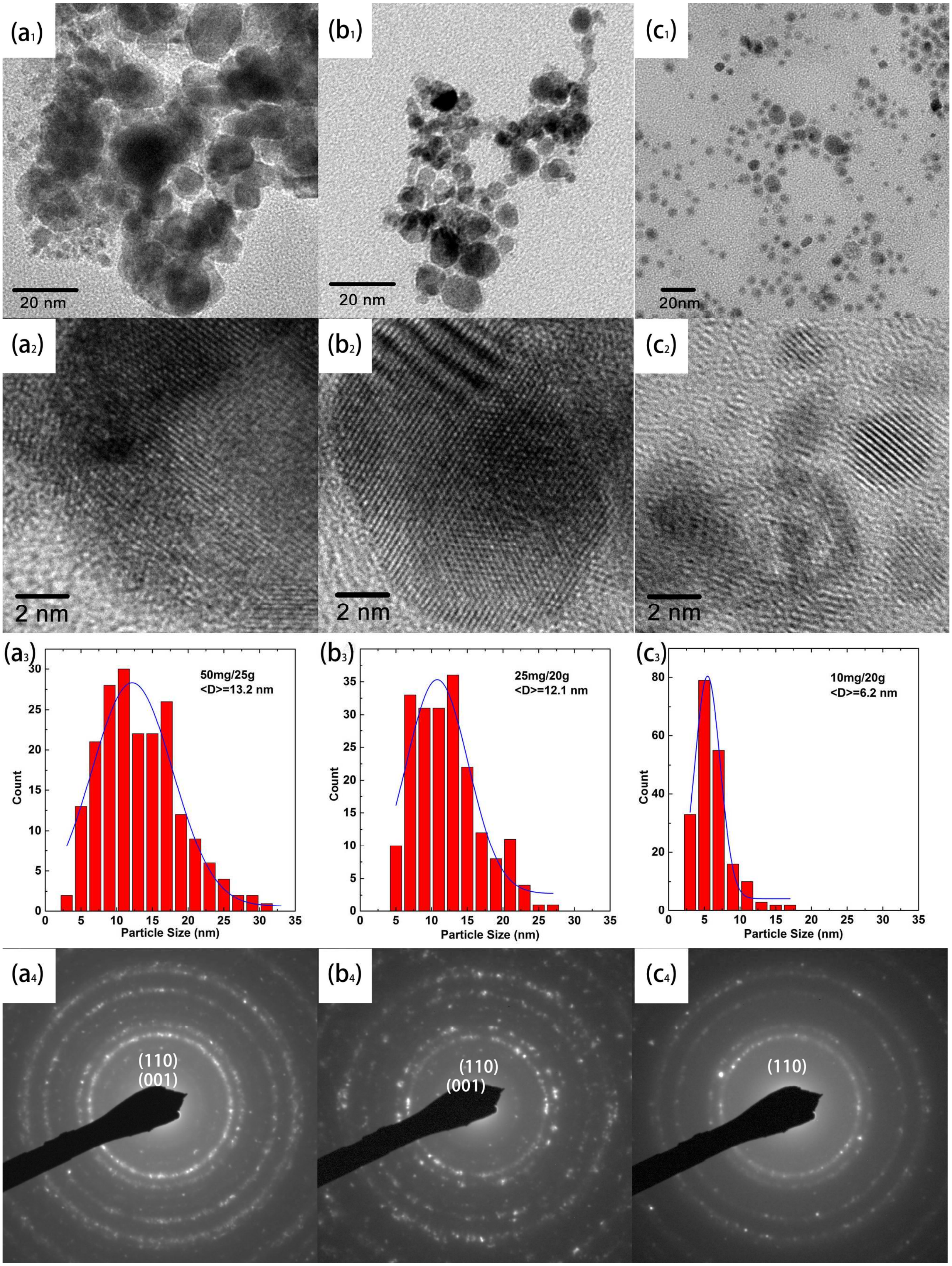

Figure 4. (a_1) bright-field image of sample S50 (a_2) high resolution image of sample S50 (a_3) size distribution of sample S50 (a_4) diffraction pattern of S50 (b_1) bright-field image of sample S25 (b_2) high resolution image of sample S25 (b_3) size distribution of sample S25 (b_4) diffraction pattern of S25 (c_1) bright-field image of sample S10 (c_2) high resolution image of sample S10 (c_3) size distribution of sample S10 (c_4) diffraction pattern of sample S10.

The degree of chemical ordering of FePt NPs can be quantified y the long-range ordering parameter S, which can be calculated by the following formula:

$$S = \left[\left(\frac{I_{001}}{I_{002}}\right)\left(\frac{F_f}{F_s}\right)^2 \frac{(L \times A \times D)_f}{(L \times A \times D)_s}\right]^{\frac{1}{2}} \cong 0.85\left(\frac{I_{001}}{I_{002}}\right)^{\frac{1}{2}} \qquad (1)$$

where I_{hkl} is the integrated intensity, F the structure factor, L the Lorentz polarization factor, A the absorption factor, D the temperature factor, and the subscripts f and s refer to the fundamental and superlattice peaks respectively.[25] According to formula (1), the ordering parameter for sample S50 is 0.75, which is high for chemically synthesized FePt NPs. For sample S25 and S10, the ordering parameter is 0.75 and 0.53.

The TEM images of FePt NPs are shown in Fig. 4. For the sample S50 the bright-field images show a size distribution (see Fig. 4a$_1$) in the range 5 - 35 nm (Fig. 5a$_3$). All the observed NPs are single crystals as shown from the high-resolution TEM (HRTEM) images in Fig. 4a$_2$. Some coalescence is present, indicating that the concentration of $[Fe(H_2O)_6]PtCl_6$ in NaCl was too high for this sample to ensure a good separation of the nanocrystals precursor. The (100) and (110)) characteristic superlattice rings in the SAED pattern (Fig. 4a$_4$) confirmed that the FePt NPs have the fct structure. By decreasing the content of the precursor (sample S25) (Fig 4b$_1$) a narrower size distribution (5-23 nm) was obtained (Fig 4b$_3$). Actually, the majority of the NPs have a size in the range 5-15 nm and only a few NPs larger than 20 nm were observed. A certain degree of coalescence was also observed (Fig. 4b$_1$). In this sample, the nanoparticles are also single crystals (Fig. 4b$_2$, 4b$_4$) and with the fct structure. Better results were achieved in sample S10. In Fig 4c$_1$ we can see well-separated NPs in the range 3-6 nm with only few NPs out of it. In this sample we did not observe coalescence phenomena, the NPs remaining always well separated. The HRTEM images (Fig. 4c$_2$) always confirm the presence of single crystal NPs and SAED pattern (Fig. 4c$_4$) together with XRD (Fig. 3$_{S10}$) confirmed the fct structure. The Standard deviation of size distributions is reported, for convenience, in the summary table.

Fig. 5 shows the magnetization data for the three samples. The magnetization curves at 30 kOe (maximum field used) are far from saturation because of the large magnetocrystalline anisotropy of the fct phase and the randomness of the particles. The highest coercivity is obtained in the particles with the largest average grain size (13.2 nm). As expected, the coercive field increases at lower temperature, from 10.9 kOe (RT) to 15.7 kOe (50 K) for sample S50 (Fig.5a), from 4.7 kOe (RT) to 4.8 kOe (50K) for sample S10 (Fig. 5c), with the largest variation from 5.2 kOe (RT) to 10.3 kOe (50 K) observed in sample S25 (Fig. 5b). The shape of the hysteresis loops and the value of coercivity suggest the presence of two contributions to the magnetization curves. The variation of Hc with the decrease of dimension in a magnetic nanoparticle system is well understood. Going from the multidomain regime (bigger particles) toward smaller particles, the coercivity first increases to a maximum, at the single domain region, and then decreases with size reduction because of thermal effects. Below a critical size, different for each material, the coercivity becomes zero and the system enters the so-called superparamagnetic state, where thermal effects are predominant making the magnetization unstable. For L1$_0$ FePt nanoparticles

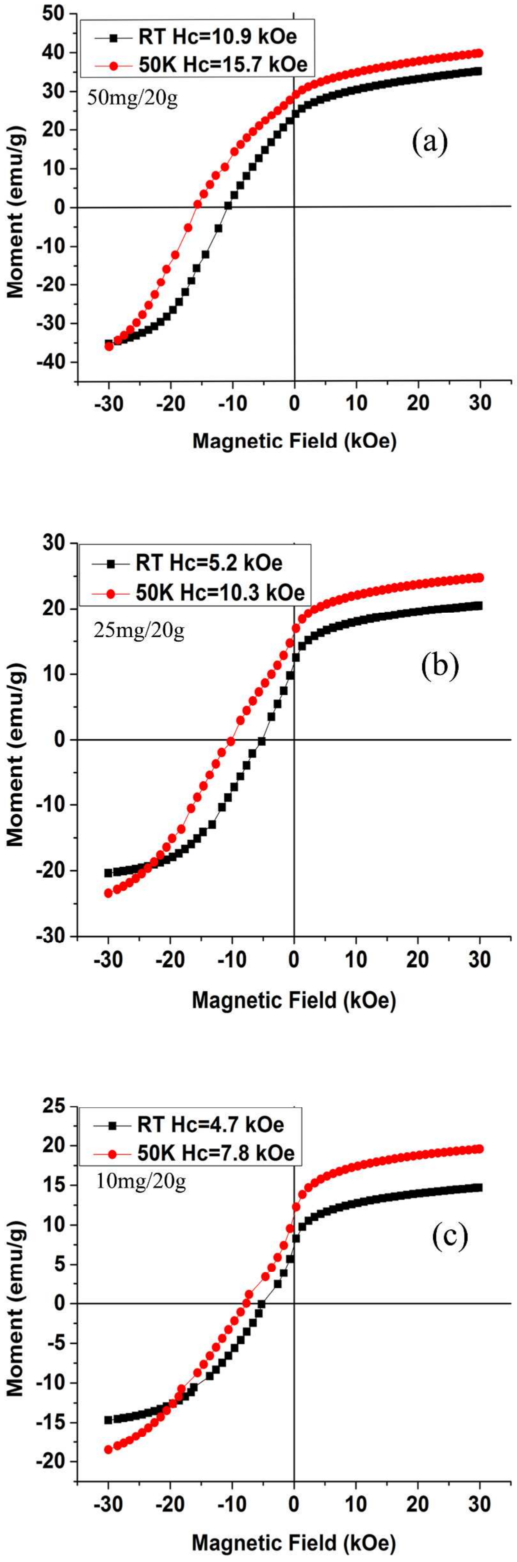

Figure 5. Hysteresis loops of the samples (a)S50, (b) S25 and (c) S10 at room temperature and T = 50 K

the superparamagnetic limit at room temperature (RT) is 2.8 nm, then, we can argue that in our nanoparticle systems both contributions, coming from single domain ferromagnetic NPs and superparamagnetic NPs with size below 2.8 nm, are present. The decrease of coercivity observed going from sample S50 to sample S10 can be explained by the particle size reduction below the single domain region. Moreover, the shape of the magnetization curves can be explained by two contributions, one coming from the bigger hard NPs with size > 2.8 nm and the other one from soft, superparamagnetic NPs with diameter smaller than 2.8 nm. Indeed, sample S10 shows the highest percentage of smaller nanoparticles with respect to the other two samples. The increasing contribution from soft superparamagnetic nanoparticles in this sample is also confirmed by the loops measured at different temperatures, where a very small difference of coercivity from RT and 50 K is observed.

Conclusions

In this work, the authors describe a green synthesis of FePt NPs with the $L1_0$ structure. To the best of our knowledge this is the first time that magnetically hard NPs are synthesized using only environmentally friendly chemical products like water and sodium chloride. By planetary ball milling of the $[Fe(H_2O)_6]PtCl_6$ precursor and NaCl and subsequent annealing at 400 °C (250 °C less than the typical temperature) in reducing atmosphere, we obtained FePt $L1_0$ NPs with selected size as a function of $[Fe(H_2O)_6]PtCl_6$ / NaCl ratio. By varying this ratio, we were able to avoid the coalescence phenomena and obtain single crystal NPs with size around 6 nm. This method in principle could be used, starting from other bimetallic salts, to carry out environmentally friendly synthesis of many other bimetallic chemically ordered alloys as AuCu, CoPt, etc. applicable in fields as magnetism and catalysis.

Aknowledgements

This work was supported by DOE DE-FG02-04ER4612 and PIRSES-GA-2011-295190 project.

Notes and references

[a] *Department of Materials Science and Engineering, University of Delaware, DE, USA .*
[b] *Istituto di Struttura della Materia. CNR, Roma, Italy. Via Salaria Km 29.300, 00015, cp10, Monterotondo (ROMA). Fax:+390690672327; Tel: +390690672554; E-mail:aldo.capobianchi@ism.cnr.it*
[c] *Department of Physics and Astronomy, University of Delaware, DE, USA,*
DOI: 10.1039/b000000x/

1. H. W. Zhang, Y. Liu and S. H. Sun, *Front Phys China*, 2010, **5**, 347-356.
2. B. Balamurugan, D. J. Sellmyer, G. C. Hadjipanayis and R. Skomski, *Scripta Mater*, 2012, **67**, 542-547.
3. A. Mari, E. Agostinelli, D. Fiorani, A. Flamini, S. Laureti, D. Peddis, A. M. Testa, G. Varvaro, M. V. Mansilla, A. Mezzi and S. Kaciulis, *Superlattice Microst*, 2009, **46**, 95-100.
4. A. Akbarzadeh, M. Samiei and S. Davaran, *Nanoscale Res Lett*, 2012, **7**, 1-13.
5. K. Inomata, T. Sawa and S. Hashimoto, *J Appl Phys*, 1988, **64**, 2537-2540.
6. J. P. Wang, *P Ieee*, 2008, **96**, 1847-1863.
7. T. Miyazaki, O. Kitakami, S. Okamoto, Y. Shimada, Z. Akase, Y. Murakami, D. Shindo, Y. K. Takahashi and K. Hono, *Phys Rev B*, 2005, **72**.
8. S. D. Bader, *Rev Mod Phys*, 2006, **78**, 1-15.
9. Y. Itoh, T. Aoyagi, A. Tsukamoto, K. Nakagawa, A. Itoh and T. Katayama, *Jpn J Appl Phys 1*, 2004, **43**, 8040-8043.
10. S. H. Sun, C. B. Murray, D. Weller, L. Folks and A. Moser, *Science*, 2000, **287**, 1989-1992.
11. S. H. Sun, *Adv Mater*, 2006, **18**, 393-403.
12. P. Gibot, E. Tronc, C. Chaneac, J. P. Jolivet, D. Fiorani and A. M. Testa, *J Magn Magn Mater*, 2005, **290**, 555-558.
13. Q. Dong, G. J. Li, C. L. Ho, M. Faisal, C. W. Leung, P. W. T. Pong, K. Liu, B. Z. Tang, I. Manners and W. Y. Wong, *Adv Mater*, 2012, **24**, 1034-1040.
14. M. Nakaya, M. Kanehara, M. Yamauchi, H. Kitagawa and T. Teranishi, *J Phys Chem C*, 2007, **111**, 7231-7234.
15. W. C. Wen, R. V. Chepulskii, L. W. Wang, S. Curtarolo and C. H. Lai, *Acta Mater*, 2012, **60**, 7258-7264.
16. V. Tzitzios, G. Basina, L. Colak, D. Niarchos and G. Hadjipanayis, *J Appl Phys*, 2011, **109**, 07A718.
17. M. Nakaya, M. Kanehara and T. Teranishi, *Langmuir*, 2006, **22**, 3485-3487.
18. M. S. Wellons, W. H. Morris, Z. Gai, J. Shen, J. Bentley, J. E. Wittig and C. M. Lukehart, *Chem Mater*, 2007, **19**, 2483-2488.
19. A. Capobianchi, M. Colapietro, D. Fiorani, S. Foglia, P. Imperatori, S. Laureti and E. Palange, *Chem Mater*, 2009, **21**, 2007-2009.
20. A. Capobianchi, G. Campi, M. Camalli and C. Veroli, *Z Kristallogr*, 2009, **224**, 384-388.
21. S. N. Hsiao, S. H. Liu, S. K. Chen and H. Y. Lee, *Ieee T Magn*, 2012, **48**, 4014-4017.
22. Y. Endo, N. Kikuchi, O. Kitakami and Y. Shimada, *J Appl Phys*, 2001, **89**, 7065-7067.
23. V. R. Reddy, S. Kavita and A. Gupta, *J Appl Phys*, 2006, **99**.
24. H. M. Song, J. H. Hong, Y. B. Lee, W. S. Kim, Y. Kim, S. J. Kim and N. H. Hur, *Chem Commun*, 2006, 1292-1294.
25. J. A. Christodoulides, P. Farber, M. Daniil, H. Okumura, G. C. Hadjipanayis, V. Skumryev, A. Simopoulos and D. Weller, *Ieee T Magn*, 2001, **37**, 1292-1294.